PAPER

Check for updates

A stimuli-responsive polymer modified nanopore for measuring β-amyloid peptide and zinc ions in brains of live mice with Alzheimer's disease†

Shushu Ding, [ID] [ab] Yue Zhu,[a] Anwei Zhu [ID] [b] and Guoyue Shi [ID] *[b]

β-Amyloid peptide (Aβ) monomers and zinc ions (Zn^{2+}) are closely related with Alzheimer's disease (AD). Sensitive and selective monitoring of Aβ monomers and Zn^{2+} in the cerebral nervous system can provide important insights into the pathological process of AD. Herein, we report the development of a single glass nanopore product based on a novel four-component stimuli-responsive copolymer for the recognition of both Aβ monomers and Zn^{2+}. Introduction of Aβ monomers appeared to have induced a change in the conformation of the copolymer, with this change leading to a significant regulation of the ion flux within the nanopore channel. Benefiting from its capacity to form multiple hydrogen-bonding interactions, the developed nanopore product displayed good sensitivity and selectivity for Aβ monomers. In addition, carboxamidoquinoline with an alkoxyethylamino chain (AQZ) was incorporated into the copolymer chains for the detection of Zn^{2+} through coordination bonds. This method was found to be ultra-sensitive for Aβ monomers and Zn^{2+}, with detection limits down to 0.1 pM and 0.1 nM. As a result, when combined with *in vivo* microdialysis, this remarkably performing glass nanopore was successfully utilized for evaluating Aβ monomer and Zn^{2+} levels in the cerebrospinal fluid (CSF) of live mice.

1. Introduction

As a neurodegenerative disorder, Alzheimer's disease (AD) is the most common type of dementia. The diagnosis and treatment of AD is challenging due to the complexity of the mechanism of its pathology.[1,2] β-Amyloid peptide (Aβ) monomers cleaved from the amyloid precursor protein have been observed in cerebrospinal fluid (CSF). They tend to aggregate into toxic fibrils during the progression of AD. Therefore, the quantity of Aβ monomers (especially for $Aβ_{1-40}$ and $Aβ_{1-42}$) in CSF has been considered to be a key predictor of AD.[3–5] On the other hand, metal ions such as the zinc ion (Zn^{2+}) have been proposed to be closely implicated in the pathogenesis of AD. Zn^{2+} is capable of directly binding to Aβ and contributes to the assembly of fibrils.[6–8] Therefore, it would appear to be highly important to monitor the levels of both Aβ monomers and Zn^{2+}, in particular for advancing our understanding of the pathogenesis of AD.

Recently, considerable efforts have been devoted to developing methods for detecting Aβ monomers or Zn^{2+}.[9–13] The use of glass-capillary-based nanopores has become a powerful analytical technique with high sensitivity.[14–18] Long *et al.* reported the use of a glass nanopore to monitor the dynamic aggregation of $Aβ_{1-42}$ peptide, but this sensor mostly relied on the resistance-pulse technique (*i.e.*, *i–t* trace), which presented a great challenge for the analysis in complex conditions because the tiny pore was easily blocked.[19] More importantly, there have been hardly any reports on the use of a single biosensor to detect both Aβ monomers and Zn^{2+}.

In the current work, we developed a glass nanopore product for the detection of Aβ monomers and Zn^{2+} with high sensitivity and selectivity. Here, a four-component copolymer was integrated into the inner surface of a glass nanopore (Scheme 1). Inspired by a role of sialic acid (SA) on cell membranes in living systems—specifically the presentation of SA as clusters on cell membranes being able to promote the deposition of Aβ with multivalent interactions[20–22]—SA in our current work was covalently grafted onto the polymer chains of the four-component copolymer for highly sensitive detection of Aβ monomers. The polymers provided abundant recognition sites, which promoted the binding of targets. Through synergetic hydrogen-bonding interactions, a swelling–producing change in conformation occurred in the presence of Aβ monomers,

[a] *School of Pharmacy, Nantong University, 19 Qixiu Road, Nantong 226001, People's Republic of China*
[b] *School of Chemistry and Molecular Engineering, Shanghai Key Laboratory for Urban Ecological Processes and Eco-Restoration, East China Normal University, 500 Dongchuan Road, Shanghai 200241, People's Republic of China. E-mail: gyshi@chem.ecnu.edu.cn; Fax: +86 21 54340043; Tel: +86 21 54340043*

† Electronic supplementary information (ESI) available. See DOI: https://doi.org/10.1039/d2sd00228k
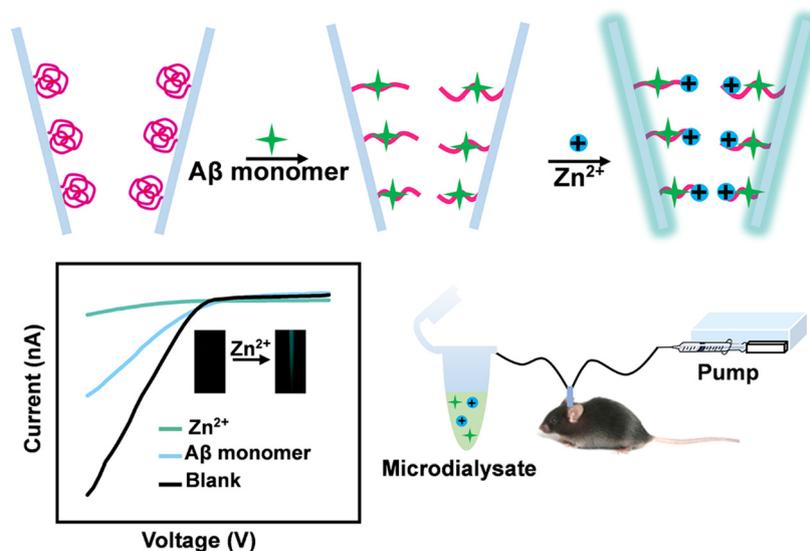
Scheme 1 Schematic of the process involving the use of the copolymer-modified glass nanopore combined with microdialysis for assaying cerebral Aβ monomers and Zn^{2+}.

leading to a decrease of the nanochannel diameter and blockage of ion flux. Taking advantage of the programmability of stimuli-responsive polymers, carboxamidoquinoline with an alkoxyethylamino chain (AQZ) was incorporated into the polymer chains. The stretching of the copolymers benefited the access and enrichment of Zn^{2+}, and AQZ could bind Zn^{2+} using coordination bonds. The specific interaction between Zn^{2+} and copolymer not only altered surface charges and triggered an ionic current response but also enhanced the fluorescence of the copolymers in the glass nanopore product. The nanopore platform with dual signals provides additional corrections to the results of methods using only a single signal, leading to an improvement in the accuracy of the analytical method. These significant properties enabled the glass nanopore product to be used, together with microdialysis, to evaluate Aβ monomers and Zn^{2+} in live mice displaying AD. To the best of our knowledge, this is the first report of a development of stimuli-responsive copolymer-modified glass nanopore for monitoring the changes of both Aβ monomer and Zn^{2+} levels associated with AD.

2. Results and discussion

2.1 Characterization of PNI-TP-SA-AQZ

As a starting point for this work, a SA derivative and quinoline derivative (AQZ) were synthesized and characterized (ESI,† Fig. S1–S6). On the basis of the "recognition-mediating-function" (RMF) design concept, a novel stimuli-responsive polymer with four components (PNI-TP-SA-AQZ) was synthesized by carrying out reversible addition–fragmentation chain transfer (RAFT) (Fig. S7†). Fourier-transform infrared spectroscopy (FT-IR) and nuclear

magnetic resonance (^{1}H NMR) were employed to characterize the composition of PNI-TP-SA-AQZ. As shown in Fig. S8,† the typical absorption of the C=O of the acetyl group of the SA unit was observed at 1731 cm^{-1}, while the signals for the C=S and C–F vibrations in the TP unit appeared at 1135 and 1279 cm^{-1}. And the signal for the stretching vibration of the secondary amine (N–H) in the AQZ unit was observed at 3335 cm^{-1}. Signals also appeared at 2935 and 2974 cm^{-1}, and were attributed to the stretching vibration of –CH_3 in the PNI unit. Moreover, the signal observed for the monomer reactants at 1731 cm^{-1} was not observed for the product, and instead there was an enhancement of the signal at 3335 cm^{-1}, demonstrating the deprotection of acetyl groups and the introduction of hydroxyl groups. These results demonstrated the successful polymerization of the four monomers, which was further confirmed using ^{1}H NMR (Fig. S9†).

2.2 Characterization of copolymer-functionalized glass nanopores

The glass nanopore was firstly fabricated (Fig. 1A). An SEM image of the nanopore showed a 70 nm diameter for its tip (Fig. S10†). Then, gold film was coated on the inner surface of the nanochannel by following a facile photochemical route. As shown in Fig. S11A,† the gold film uniformly covered the tip of the nanopore. When under electron beam irradiation, the middle of the nanopore showed at times relatively transparent bubbles due to irradiation-induced melting of the ultrathin gold film. Meanwhile, distinct peaks corresponding to Au were clearly seen in the EDX spectrum acquired from the modified nanopore (Fig. S11B†). The Au coating yielded an increased ionic current at −1 V ($I_{-1.0V}$), due to strong adsorption of Cl^- onto the Au surface.[23] Finally, the
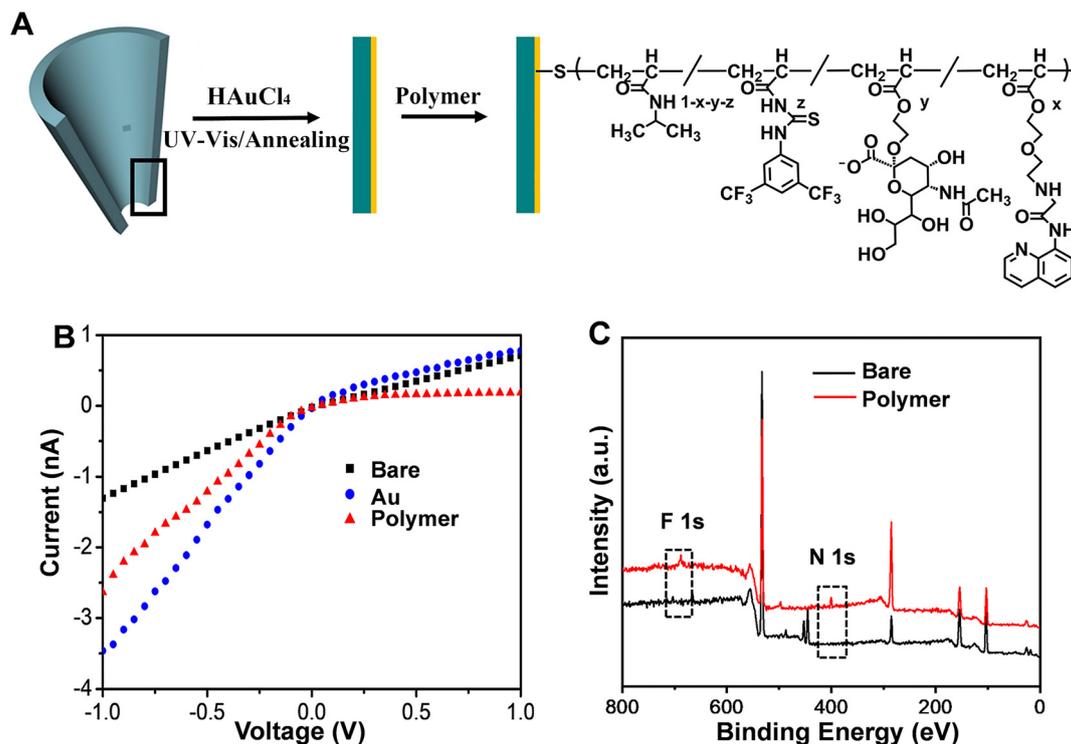
Fig. 1 (A) Process used for fabricating the copolymer-modified glass nanopore. (B) I–V curves of the bare, Au-modified and copolymer-modified glass nanopore. (C) XPS spectra of the bare glass slide and copolymer-modified glass slide.

copolymer PNI-TP-SA-AQZ was grafted onto the inner surface of the glass nanopore based on the formation of Au–S bonds; this process resulted in a decrease of $I_{-1.0V}$ (Fig. 1B). An X-ray photoelectron spectrometry (XPS) analysis showed an appearance of F 1s (688.2 eV) and N 1s (399.1 eV) peaks upon the modification with the copolymer (Fig. 1C). These results validated the successful fabrication of copolymer-modified glass nanopore.

2.3 Electrochemical response of copolymer-modified glass nanopores

We next investigated the response of the synthesized copolymer-modified glass nanopore to Aβ monomers. As shown in Fig. 2A, the $I_{-1.0V}$ gradually declined in response to increasing concentrations of Aβ monomers. The relative current change ($|(I - I_0)/I_0|$, where I_0 represents the ionic current without Aβ treatment) at −1.0 V showed a good linearity with the logarithm of the concentration of Aβ monomers for concentrations between 10^{-13} M and 10^{-9} M $[y = 1.8894 + 0.1343 \log x \ (R^2 = 0.9964)]$ (Fig. 2B). The detection limit was lower than 10^{-13} M, better than those of other reported methods (Table S1†). As a stimuli-responsive polymer, the phase transition can be easily adjusted due to the PNIPAAm chains having variable hydrogen-bonding environments.[24–26] As shown in Fig. 2C, the copolymer showed a film thickness of ∼12 nm. After being treated with the Aβ monomer solution, the film

swelled, with an increase of its thickness to ∼25 nm (Fig. 2D).

In view of the above results, we derived an explanation for the decrease in the ionic current of the copolymer upon its exposure to Aβ monomers. According to this proposal, in the presence of Aβ monomers, the SA unit interacted with Aβ monomers through multiple hydrogen bonds,[20,27–31] which can be further enhanced by the TP unit. Hence, the intramolecular hydrogen bonds within the copolymer chains were broken. As a result, the copolymer film became stretched and the effective radius of the nanopore decreased, which hindered the ion transport in the nanochannel.[32]

Although the presence of Aβ monomers triggered a change in the wettability of the polymeric film (Fig. S12†), the change in the conformation of the polymer chains was the predominant factor that caused the decrease of the ionic current. The effects of the concentration of copolymer and UV light irradiation time on the ionic current were investigated (Fig. S13†). In addition, the ionic current responses of six different nanopores to Aβ monomer solution (10^{-9} M) showed a relative standard deviation of only 2.2% (Fig. S14†), revealing a good reproducibility of the fabrication and properties of the copolymer-modified glass nanopore.

Subsequently, the glass nanopores exposed to Aβ monomers were utilized for detecting Zn^{2+}. Previous reports have shown that AQZ binds Zn^{2+} with coordination bonds (Fig. 3A),[33] and that upon treatment of AQZ with Zn^{2+}, the intramolecular hydrogen bond in AQZ becomes broken,
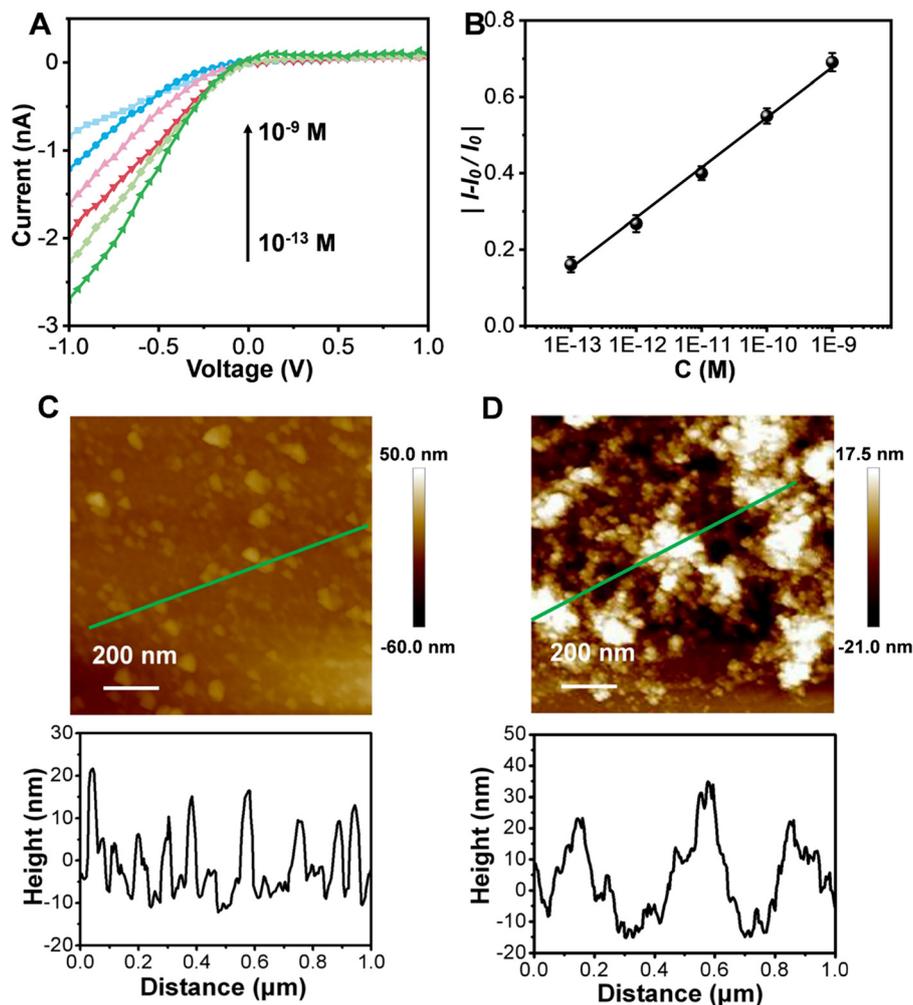
Fig. 2 (A) *I–V* curves of copolymer-modified glass nanopores treated with Aβ monomers of different concentrations (10^{-13} M, 10^{-12} M, 10^{-11} M, 10^{-10} M, 10^{-9} M). (B) Calibration curve for relative current change *vs.* the logarithm of the concentration of Aβ monomers. (C and D) AFM images of the copolymer decorated on the Au surface (C) before and (D) after the Au surface was treated with a solution of Aβ monomers, and corresponding cross-section analyses along the green lines in the images.

which can stop intramolecular electron transfer, leading to enhancement of fluorescence emission.[34,35] Therefore, we next investigated the fluorescence response of the copolymer to Zn^{2+}. As shown in Fig. 3B, the nanopore tip showed a blue-green fluorescence emission upon its exposure to Zn^{2+}. More interestingly, the $I_{-1.0V}$ gradually decreased with an increase in Zn^{2+} concentration (Fig. 3C); this decrease in current was attributed to a decrease in the number of negative surface charges. Fig. 3D displays a plot of the relative change in current *versus* the logarithm of concentration of Zn^{2+} [$y = 1.8026 + 0.16121 \log x$ ($R^2 = 0.9991$)]. The detection limit for Zn^{2+} was as low as 10^{-10} M. These results indicated that the platform could realize dual-signal detection of Zn^{2+}, which can provide an additional correction to the results from using a single signal, hence improving the accuracy of the analytical method. In addition, the ability of the Aβ-monomer-exposed copolymers to recognize Zn^{2+} may be attributed to an Aβ-monomer-induced swelling–producing

conformational transition of the copolymer chains having promoted the access and enrichment of Zn^{2+}. This is, to the best of our knowledge, the first report of a single glass nanopore being applied for the recognition of both Aβ monomers and Zn^{2+}.

Since selectivity is of great importance for detecting biomolecules in brain systems, we set out to investigate any interference in our developed detection system from coexisting biomolecules, including some proteins, amino acids, metal ions and other biological species. As shown in Fig. S15,† there were low responses from other proteins except for Aβ oligomer, while Aβ monomer displayed a significant response. Note that the issue of Aβ oligomer can be addressed by using microdialysis and a probe with an appropriate molecular weight cut-off to remove Aβ oligomer from biological samples. Meanwhile, negligible signals were obtained for amino acids, metal ions and other biological species. Selectivity for Zn^{2+} was also investigated. Other metal ions showed no obvious
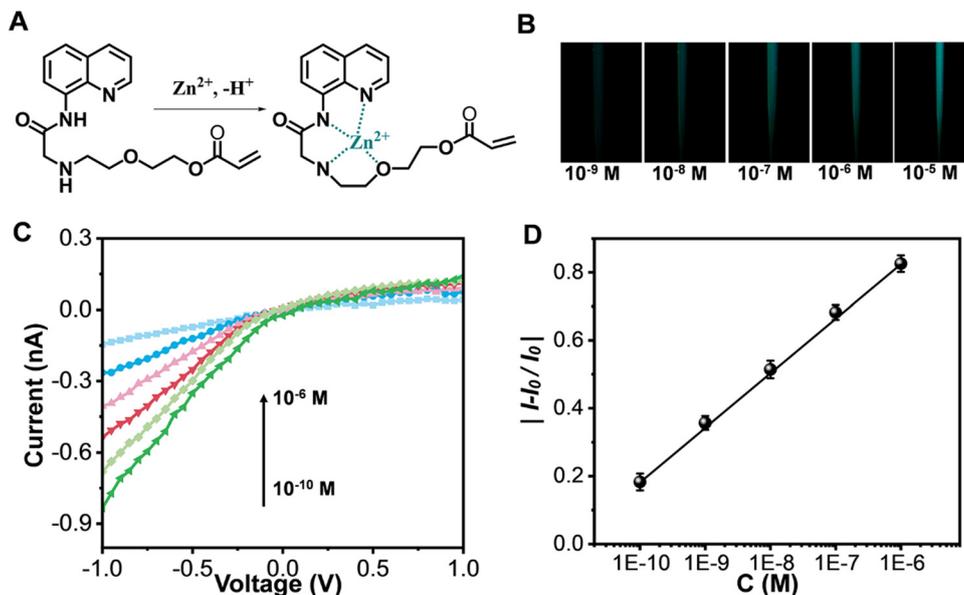
Fig. 3 (A) Chemical structure depiction of the reaction of AQZ with Zn^{2+}. (B) Fluorescence images and (C) *I–V* curves obtained of Aβ-copolymer-modified nanopores treated with indicated concentrations of Zn^{2+}, λ_{ex} = 365 nm. (D) Calibration curve for relative current change *vs.* the logarithm of Zn^{2+} concentration.
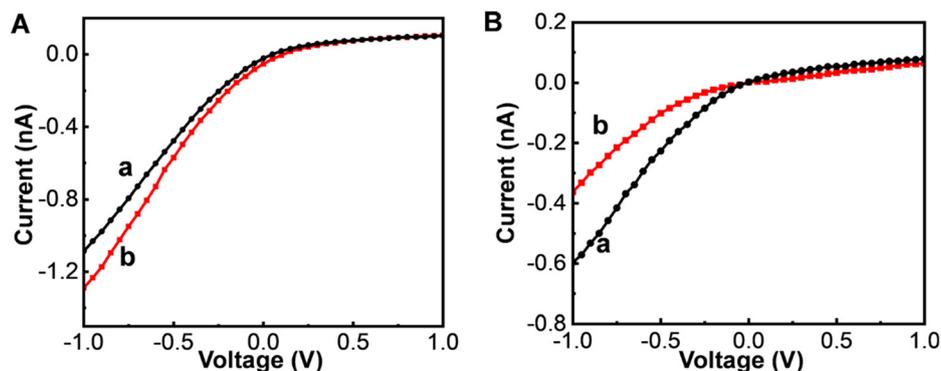

Fig. 4 *I–V* curves obtained at the (A) copolymer-modified glass nanopore for determination of the concentration of Aβ monomers and (B) Aβ-copolymer-modified glass nanopore for determination of the concentrations of Zn^{2+} in CSFs of normal (a) and AD mice (b).

responses. Moreover, proteins, amino acids and other biological species demonstrated little interference with the detection of Zn^{2+}. In competition tests, the electrochemical responses to Aβ monomers and Zn^{2+} were hardly affected by the addition of the above biomolecules. All these results demonstrated high selectivity of the developed glass nanopore for the recognition of Aβ monomers and Zn^{2+}.

2.4 Monitoring Aβ monomers and Zn^{2+} in mouse cerebrospinal fluid

We took advantage of the high sensitivity and selectivity of the glass nanopore product by applying it to further monitor Aβ monomer and Zn^{2+} levels in cerebrospinal fluid (CSF). Fig. 4A shows electrochemical responses to Aβ monomers in normal (curve a) and AD (curve b) mice. The $I_{-1.0V}$ for the

Table 1 Concentrations of Aβ monomer and Zn^{2+} in the CSFs of normal and AD mice determined using the present method

Disease status	Aβ monomer				Zn^{2+}			
	Mouse 1	Mouse 2	Mouse 3	Mean ± SD	Mouse 1	Mouse 2	Mouse 3	Mean ± SD
Normal	3.83 nM	3.93 nM	4.08 nM	3.95 ± 0.13 nM	6.43 nM	6.57 nM	6.28 nM	6.43 ± 0.15 nM
AD	1.07 nM	1.08 nM	1.12 nM	1.09 ± 0.03 nM	0.35 μM	0.31 μM	0.43 μM	0.36 ± 0.06 μM

mouse brain with AD was higher than that in the normal brain. According to the microdialysis recovery (6%) and calibration curve, the concentrations of Aβ monomers in the CSFs of the normal and AD mice were estimated to be 3.95 ± 0.13 nM and 1.09 ± 0.03 nM, respectively. As shown in Fig. 4B, the concentrations of Zn^{2+} in the CSFs of the normal and AD mice were calculated to be 6.43 ± 0.15 nM and 0.36 ± 0.06 μM, respectively. That is, in comparison to their levels in the brains of normal mice, the level of Aβ monomers was ~3.6-fold lower and that of Zn^{2+} ~ 56-fold higher in the brains of mice with AD (Table 1). These results were consistent with the ability of synaptic vesicles to release large amounts of Zn^{2+} during AD pathogenesis, a feature contributing to Aβ deposition.[36,37]

3. Conclusions

In summary, we developed a glass nanopore product based on a novel four-component stimuli-responsive copolymer for detecting both Aβ monomers and Zn^{2+} with high sensitivity and selectivity. The remarkable analytical performance of this glass nanopore enabled it to be used to investigate the physiological/pathological changes in neurodegenerative diseases. By combining use of the nanopore with microdialysis, this study has shown the ability to monitor changes in the levels of Aβ monomers and Zn^{2+} in the brains of living mice with or without AD, and hence has contributed to the development of a deep understanding of the mechanism of the AD pathology. By easily changing the copolymer structure using the "RMF" design principle, this work has also proposed a methodology for designing stimuli-responsive polymer-based glass nanopores for monitoring other biomolecules related to brain disease.

Author contributions

Shushu Ding: investigation, methodology, data curation, writing – original draft, funding acquisition. Yue Zhu: methodology, data curation. Anwei Zhu: writing – review & editing, funding acquisition, resources. Guoyue Shi: funding acquisition, resources.

Conflicts of interest

There are no conflicts to declare.

Acknowledgements

References

1 M. J. Oset-Gasque and J. Marco-Contelles, *ACS Chem. Neurosci.*, 2018, **9**, 401–403.

2 M. H. Murdock and L. H. Tsai, *Nat. Neurosci.*, 2023, **26**, 181–195.

3 Y. Y. Yu, L. Zhang, C. L. Li, X. Y. Sun, D. Q. Tang and G. Y. Shi, *Angew. Chem., Int. Ed.*, 2014, **53**, 1–5.

4 T. Hu, C. X. Chen, G. M. Huang and X. R. Yang, *Sens. Actuators, B*, 2016, **234**, 63–69.

5 Y. Y. Yu, X. Y. Sun, D. Q. Tang, C. L. Li, L. Zhang, D. X. Nie, X. X. Yin and G. Y. Shi, *Biosens. Bioelectron.*, 2015, **68**, 115–121.

6 P. Faller, C. Hureau and G. L. Penna, *Acc. Chem. Res.*, 2014, **47**, 2252–2259.

7 X. H. Wang, X. Y. Wang and Z. J. Guo, *Coord. Chem. Rev.*, 2018, **362**, 72–84.

8 P. Faller, C. Hureau and O. Berthoumieu, *Inorg. Chem.*, 2013, **52**, 12193–12206.

9 S. S. Ding, Y. X. Xu, Q. Liu, H. Gu, A. W. Zhu and G. Y. Shi, *Analyst*, 2020, **145**, 2331–2338.

10 C. Liu, D. K. Lu, X. R. You, G. Y. Shi, J. J. Deng and T. S. Zhou, *Anal. Chim. Acta*, 2020, **1105**, 147–154.

11 J. J. Peng, W. Xu, C. L. Teoh, S. Y. Han, B. Kim, A. Samanta, J. C. Er, L. Wang, L. Yuan, X. G. Liu and Y. T. Chang, *J. Am. Chem. Soc.*, 2015, **137**, 2336–2342.

12 N. N. Liu, R. Z. Hou, P. C. Gao, X. D. Lou and F. Xia, *Analyst*, 2016, **141**, 3626–3629.

13 W. Y. Li, B. Q. Fang, M. Jin and Y. Tian, *Anal. Chem.*, 2017, **89**, 2553–2560.

14 K. Zhang, X. He, Y. Liu, P. Yu, J. Fei and L. Mao, *Anal. Chem.*, 2017, **89**, 6794–6799.

15 J. Song, C. H. Xu, S. Z. Huang, W. Lei, Y. F. Ruan, H. J. Lu, W. Zhao, J. J. Xu and H. Y. Chen, *Angew. Chem., Int. Ed.*, 2018, **57**, 13226–13230.

16 X. L. Nie, H. L. Liu, Z. Q. Pan, S. A. Ahmed, Q. Shen, J. M. Yang, J. B. Pan, J. Pang, C. Y. Li, X. H. Xia and K. Wang, *Chem. Commun.*, 2019, **55**, 6397–6400.

17 S. S. Ding, C. Y. Liu, D. Y. Fu, G. Y. Shi and A. W. Zhu, *Anal. Chem.*, 2021, **93**, 1779–1785.

18 D. D. Wang, G. H. Qi, Y. Zhou, H. J. Li, Y. Zhang, C. Xu, P. Hu and Y. D. Jin, *Chem. Commun.*, 2020, **56**, 5393–5396.

19 R. J. Yu, S. M. Lu, S. W. Xu, Y. J. Li, Q. Xu, Y. L. Ying and Y. T. Long, *Chem. Sci.*, 2019, **10**, 10728–10732.

20 L. Lei, R. Geng, Z. A. Xu, Y. J. Dang, X. L. Hu, L. L. Li, P. Geng, Y. Tian and W. Zhang, *Anal. Chem.*, 2019, **91**, 8129–8136.

21 T. T. Yin, L. C. Yang, Y. N. Liu, X. B. Zhou, J. Sun and J. Liu, *Acta Biomater.*, 2015, **25**, 172–183.

22 J. T. Yang, Y. C. Kuo, I. Y. Chen, R. Rajesh, Y. I. Lou and J. P. Hsu, *ACS Biomater. Sci. Eng.*, 2019, **5**, 1311–1320.

23 M. Yang, C. Y. Ma, S. S. Ding, Y. J. Zhu, G. Y. Shi and A. W. Zhu, *Anal. Chem.*, 2019, **91**, 14029–14035.

24 Z. Liu, W. Wang, R. Xie, X. J. Ju and L. Y. Chu, *Chem. Soc. Rev.*, 2016, **45**, 460–475.

25 G. Y. Qing and T. L. Sun, *Adv. Mater.*, 2011, **23**, 1615–1620.

26 S. S. Ding, G. Y. Shi and A. W. Zhu, *Chem. Commun.*, 2022, **58**, 13171–13187.

27 M. Vahed, S. Neya, K. Matsuzaki and T. Hoshino, *J. Phys. Chem. B*, 2018, **122**, 3771–3781.

28 V. Wittmann and R. J. Pieters, *Chem. Soc. Rev.*, 2013, **42**, 4492–4503.

29 T. Hoshino, M. I. Mahmood, K. Mori and K. Matsuzaki, *J. Phys. Chem. B*, 2013, **117**, 8085–8094.

30 S. H. Nasr, H. Kouyoumdjian, C. Mallett, S. Ramadan, D. C. Zhu, E. M. Shapiro and X. F. Huang, *Small*, 2018, **14**, 1701828.

31 S. Hong, B. L. Ostaszewski, T. Yang, T. T. O'Malley, M. Jin, K. Yanagisawa, S. M. Li, T. Bartels and D. J. Selkoe, *Neuron*, 2014, **82**, 308–319.

32 Q. Liu, S. S. Ding, R. Gao, G. Y. Shi and A. W. Zhu, *Anal. Chim. Acta*, 2021, **1188**, 339167.

33 Y. Zhang, X. F. Guo, W. X. Si, L. H. Jia and X. H. Qian, *Org. Lett.*, 2008, **10**, 473–476.

34 Y. C. Chen, Y. Bai, Z. Han, W. J. He and Z. J. Guo, *Chem. Soc. Rev.*, 2015, **44**, 4517–4546.

35 Z. Xu, K. H. Baek, H. N. Kim, J. Cui, X. Qian, D. R. Spring, I. Shin and J. Yoon, *J. Am. Chem. Soc.*, 2010, **132**, 601–610.

36 L. Wang, Y. L. Yin, X. Z. Liu, P. Shen, Y. G. Zheng, X. R. Lan, C. B. Lu and J. Z. Wang, *Transl. Neurodegener.*, 2020, **9**, 10.

37 S. D. Portbury and P. A. Adlard, *Int. J. Mol. Sci.*, 2017, **18**, 2506.